Studying femtosecond-laser hyperdoping by controlling surface morphology

Mark T. Winkler,[1,a)] Meng-Ju Sher,[1] Yu-Ting Lin,[2] Matthew J. Smith,[3] Haifei Zhang,[2] Silvija Gradečak,[3] and Eric Mazur[1,2,b)]

[1]*Department of Physics and School of Engineering and Applied Sciences, Harvard University, 9 Oxford Street, Cambridge, Massachusetts 02138, USA*

[2]*School of Engineering and Applied Sciences, Harvard University, 9 Oxford Street, Cambridge, Massachusetts 02138, USA*

[3]*Department of Materials Science and Engineering, Massachusetts Institute of Technology, 77 Massachusetts Ave., Cambridge, Massachusetts 02139, USA*

(Received 11 November 2011; accepted 30 March 2012; published online 4 May 2012)

We study the fundamental properties of femtosecond-laser (fs-laser) hyperdoping by developing techniques to control the surface morphology following laser irradiation. By decoupling the formation of surface roughness from the doping process, we study the structural and electronic properties of fs-laser doped silicon. These experiments are a necessary step toward developing predictive models of the doping process. We use a single fs-laser pulse to dope silicon with sulfur, enabling quantitative secondary ion mass spectrometry, transmission electron microscopy, and Hall effect measurements. These measurements indicate that at laser fluences at or above $4\,\mathrm{kJ\,m^{-2}}$, a single laser pulse yields a sulfur dose $>(3 \pm 1) \times 10^{13}\,\mathrm{cm^{-2}}$ and results in a 45-nm thick amorphous surface layer. Based on these results, we demonstrate a method for hyperdoping large areas of silicon without producing the surface roughness. © *2012 American Institute of Physics*. [http://dx.doi.org/10.1063/1.4709752]

I. INTRODUCTION

Doping bulk semiconductors with non-equilibrium concentrations of deep-level dopants—a process referred to as hyperdoping—has attracted significant interest recently as a potential route to realizing novel optoelectronic devices, including photodetectors[1,2] and intermediate band photovoltaics,[3] which are sensitive to photon energies below that of the host material's band gap. One approach to hyperdoping is to expose a silicon wafer to intense laser pulses (approximately 100 fs in duration) in the presence of ambient gaseous or solid dopant sources.[4–7] When the dopant is one of the heavy chalcogens (S, Se, and Te), the resulting doped silicon exhibits remarkable optical properties including strong absorption at photon energies well below the band gap of silicon.[4,5,8] These unique properties can be exploited to fabricate novel optoelectronic devices, such as high-gain Si photodetectors with response at photon energies as low as 0.8 eV.[1]

A predictive model of fs-laser hyperdoping does not currently exist, however, representing a challenge to designing (rather than empirically searching for) new materials using this technique. Without such a model, it is difficult to estimate the achievable combinations of microstructure, dopant profile, and dopant choice. A predictive model has not been developed, in part, because previous work has focused on treatment of silicon wafers with multiple fs-laser pulses of an intensity above the ablation threshold. Besides hyperdoping, these exposure conditions result in the development of surface features such as microspikes and nanoripples;[9] this roughened material is referred to as "black silicon."[6,7] The properties[10,11] of black silicon and its applications for optoelectronic devices[12] have been investigated. However, the superposition of laser-induced doping and surface roughness complicates understanding either effect individually. For example, surface roughness limits the quantitative accuracy in measuring the dopant distribution. Thus, no model currently exists to describe and predict the material properties (e.g., dopant profile and microstructure) of fs-laser hyperdoped materials as a function of experimental parameters (e.g., laser fluence and dopant-gas pressure)—despite the fact that predictive capability is critical for future development of functional devices based on this unique material system.

Hyperdoping can also be performed with nanosecond laser pulses;[13] in this case, predictive models have been developed, tested, and validated.[14] The lack of such models for fs-laser hyperdoping is due in part to its shorter research history and in part to the greater complexity of the process.[6] In addition to producing surface roughness, fs-laser hyperdoping relies on a laser-silicon interaction that is highly nonlinear, whereas it is linear for the ns-laser process. Regardless, fs-laser hyperdoping yields material properties distinct from other methods; for example, optoelectronic devices fabricated using fs-laser hyperdoping exhibit photoresponse at longer wavelengths and in thinner layers than those fabricated via ns-laser techniques.[1,2] A predictive model of fs-laser doping would clarify the types of new material systems and device properties that can be obtained using this technique.

In this paper, we synthesize fs-laser hyperdoped silicon free of surface roughness and investigate its fundamental structural and electronic properties, representing an initial step toward developing a descriptive model of fs-laser doping. First, we dope silicon with a single fs-laser pulse to realize and study the irreducible component of fs-laser hyperdoping.

[a)]Present address: Department of Mechanical Engineering, Massachusetts Institute of Technology, 77 Massachusetts Ave., Cambridge, Massachusetts 02139, USA.

[b)]Author to whom correspondence should be addressed. Electronic mail: mazur@seas.harvard.edu.

The surface of the samples remain unroughened and it is possible to analyze the structural and electronic properties with high accuracy using quantitative secondary ion mass spectrometry (SIMS), transmission electron microscopy (TEM), and Hall effect measurements. Second, we extend the single-pulse experiment by hyperdoping a large area ($100 \times 100\ mm^2$) of silicon such that the resulting surface is optically flat and amenable to quantitative structural characterization. This system represents a bridge between single-pulse laser doping and black silicon. These results differ from previous studies of hyperdoped Si by describing the electronic and microstructural properties resulting from exposure to single fs-laser pulses rather than complex, many-pulse exposures; further, by controlling and eliminating surface roughness, these measurements significantly improve the quantitative precision relative to previous work.

II. EXPERIMENTAL

A. Single laser-pulse doping

Si wafers are cleaned of organic and metallic surface contamination[15] and immediately transferred to a vacuum chamber which is then filled with 6.7×10^4 Pa of SF_6 gas. Except as noted, Si wafers are boron doped ($1 - 20\ \Omega \cdot cm$) and (100) orientation. Hyperdoping is performed by exposure to normally incident laser pulses from an amplified Ti:sapphire fs-laser system (average pulse energy of 2.5 mJ, center wavelength of 800 nm, and pulse duration 75 fs). Laser pulses have a Gaussian intensity profile with a fluence defined as pulse energy divided by the area of intensity greater than $1/e$ of the maximum. The pulse diameter defined by this metric is 600–1000 μm depending on the fluence used. Each experiment described below isolates a small area at the center of the laser pulse in order to achieve nearly constant fluence within the device region. By measuring the transient reflectance of a HeNe laser (632 nm) coincident on the Si surface with fs-laser pulses of varying fluence, we obtain the melting threshold and duration.

To probe the electronic role of the sulfur dopants, we measured (1) the current-voltage ($I-V$) properties of the junction between the laser-doped region and the p-type Si substrate and (2) resistivity and carrier concentration (from Hall effect measurements). The processes shown in Figure 1 were used to fabricate devices appropriate for each measurement. For $I-V$ measurements, hyperdoping was performed with a laser pulse (fluence of 8 kJ m^{-2}) centered on the exposed silicon area (step 1, Fig. 1(a)). Some samples were thermally annealed (between steps 2 and 3 of Figure 1(a)) in an open-tube furnace with a flow (280 sccm) of forming gas mixture (95% He and 5% H_2) for 30 min at 775 or 975 K. For resistivity and Hall effect measurements (Fig. 1(b)), we isolate the doped layer by hyperdoping silicon-on-insulator (SOI) wafers. The device layer of the SOI wafer was nearly undoped (n-type dopant concentration below $10^{12}\ cm^{-2}$). Using standard procedures,[16] we excited the samples with a current of less than 500 nA for both resistivity and Hall measurements. A magnetic field of 0.75 T was used for Hall measurements.

Cross-sectional TEM samples were prepared using a Zeiss NVision 40 focused ion beam. Bright-field TEM micrographs and microdiffraction patterns were collected with a JEOL 2010 F TEM operated at 200 kV. SIMS was performed on a square region ($15 \times 15\ \mu m^2$) at the center of the laser-irradiated area using a 7-keV Cs ion beam ($I_{Cs} = 10$–200 nA). Assuming singly ionized species, we monitored the ratio of atomic mass 32 to 34 during the SIMS measurement and only accepted data that matched the known isotopic abundance for

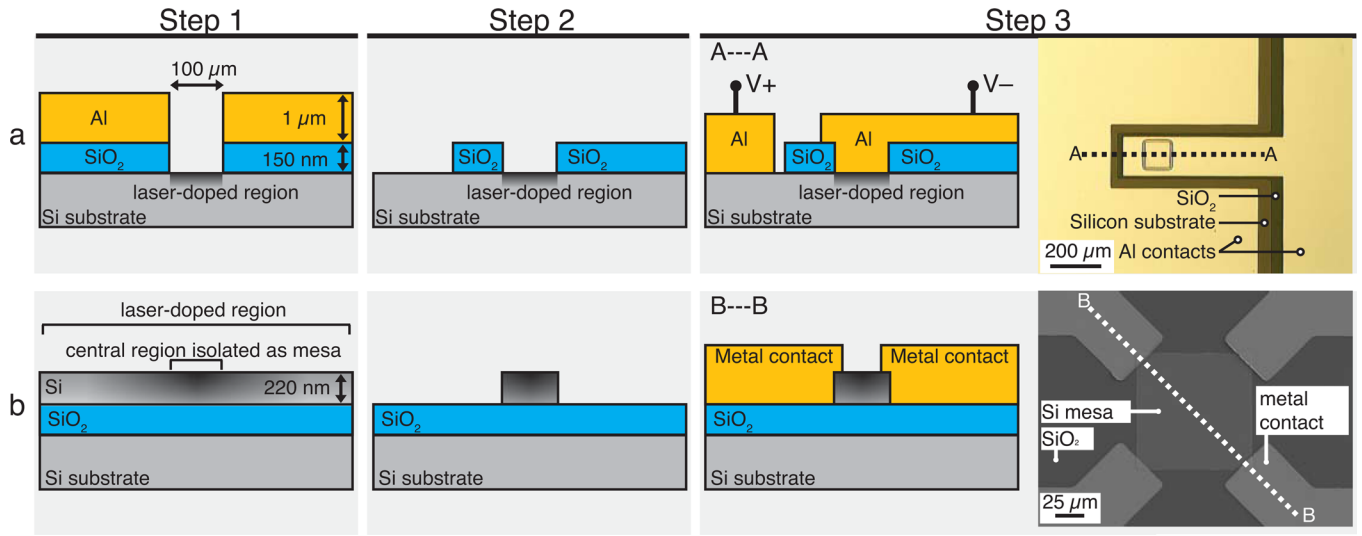

FIG. 1. Fabrication procedures. (a) To measure the *I*–*V* properties: (Step 1) a layer of thermal oxide (thickness 150 nm) was grown and a layer of Al (thickness 1 μm) was deposited atop the Si wafer; square openings ($100 \times 100\ \mu m^2$) were then etched into these layers. Hyperdoping is performed via irradiation with a single fs-laser pulse centered on the exposed area; the Al acts as a mirror, reflecting the laser pulse from the surrounding area. (Step 2) The Al is etched away; a portion of the SiO_2 layer is also etched away, leaving an insulating layer appropriate for (Step 3) deposition of Al contacts in a geometry for probing the electronic properties of the junction. The microscope image on the right shows an overhead view of the device. (b) To measure the Hall effect: (Step 1) hyperdoping is performed on a SOI wafer; afterward (Step 2), the silicon device layer is etched away except for a $100 \times 100\ \mu m^2$ area at the center of the laser-irradiated areas; finally, (Step 3) Ti/Ni/Ag contacts (20/20/500 nm) were deposited in a van der Pauw geometry.[16] An overhead scanning electron microscope image of sample prepared for Hall measurements is shown on the right.

sulfur (thus eliminating contamination from ionized O_2). Count profiles were calibrated against a known ion-implanted sample to obtain sulfur concentration versus depth.

B. Large area doping

To create large (100×100 mm^2) areas of fs-laser doped silicon, it is necessary to scan the laser across the wafer surface. Eliminating surface roughness requires a fluence and scan pattern that satisfies two conditions. First, to hyperdope the sample, all points on the surface must be melted by the laser. Second, to avoid surface roughness, no point on the surface can be exposed to a fluence above the ablation threshold. We scan the laser beam such that the centers of successive pulses strike the substrate separated by a distance d. In order to obtain a laser-treated surface with the most uniform characteristics possible, we desire a small value for d. However, some surface texture can form following laser-irradiation above the melting-threshold due to the excitation of capillary waves in the laser-melted silicon.[17] This texture can focus subsequent laser pulses inhomogeneously across the surface, increasing the fluence above the ablation threshold locally, and yielding the surface roughness observed in previous work. This constraint encourages selection of larger values of d. Experimentally, we found only a narrow window of exposure parameters that yielded both flatness and homogeneity. For the sample described below, a laser fluence $F_0 = (2 \pm 1)$ kJ m^{-2} was used, achieved by focusing a pulse with energy 140 μJ to a full-width at 1/e-maximum of 300 μm. These pulses were spaced by $d = 58$ μm.

Sample preparation for this experiment was identical to that described in Sec. II A except for the following differences. A slightly different Si substrate (phosphorus doped with $\rho \approx 1000$ Ω·cm; (111) orientation) and a different laser system (pulse energy 140 μJ and pulse duration 125 fs) were used. The laser pulses were spaced by $d = 58$ μm by reducing the laser repetition rate to a frequency $f = 11$ Hz using a mechanical shutter and translating the silicon wafer at a speed $v = 640$ μm s^{-1}. We synthesized a large sample (100×100 mm^2) and characterized it using SIMS, TEM, and atomic force microscopy (AFM).

III. RESULTS

A. Single laser-pulse doping

In order to understand how the properties of hyperdoped silicon are related to laser-process parameters such as fluence, we studied samples doped using a single laser pulse. In Figure 2(a), the sulfur concentration-depth profile is shown for various laser fluences. Sulfur is present as deep as about 50 nm in all samples before the SIMS signal becomes heavily influenced by background oxygen. Sulfur is present at larger depths for lower fluences, but the difference represents relatively little of the total sulfur content. Integrating these curves, we plot the total areal sulfur dose as a function of fluence in Figure 2(b). The shaded area indicates the detection limit, which is set by a small amount of oxygen contamination from both the vacuum chamber and the native oxide. Fluences of 3.0 and 3.5 kJ m^{-2} yield a total sulfur dose that

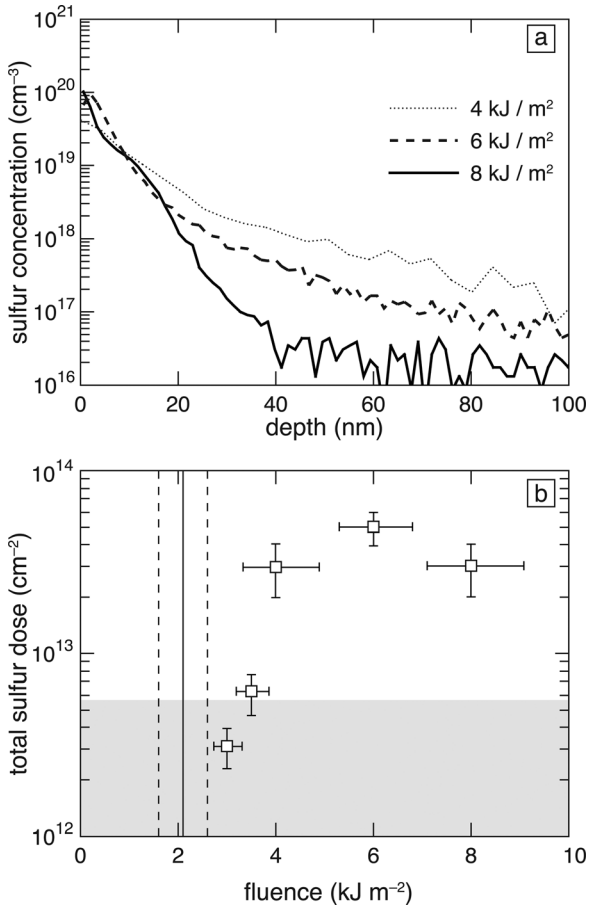

FIG. 2. (a) SIMS measurements of fs-laser doped silicon at several different fluences. (b) The implanted sulfur dose plotted against fluence indicates that sulfur is measurable above the background following irradiation with laser fluences just higher than the measured melting threshold of (2.1 ± 0.5) kJ m^{-2} (vertical lines). The shaded area indicates the detection limit of the SIMS measurement due to oxygen contamination.

is not statistically different from background, whereas samples irradiated with fluences of 4 kJ m^{-2} and higher exhibit sulfur doses an order of magnitude above this background level. Among samples with a sulfur dose above the detection limit, the total dose does not vary by more than the measurement resolution.

We measured the melting threshold of silicon irradiated as described to be $F_{melt} = (2.1 \pm 0.5)$ kJ m^{-2}; this threshold appears on Figure 2(b) as a vertical line. The melt duration is (8 ± 2) ns for 8 kJ m^{-2} fluence; the time resolution of the measurement was 1 ns, but slightly larger error bars are assigned due to the uncertainty in the fluence measurement.

From the bright-field TEM images and corresponding microdiffraction patterns of Figure 3, we find that an 8-kJ m^{-2} laser pulse creates an amorphous silicon layer extending approximately 45 nm from the surface (Figure 3(a)). A post-irradiation anneal at 975 K for 30 min drives recrystallization of the amorphous silicon layer (Figure 3(b)), and the resulting c-Si layer retains the orientation of the silicon substrate.

Table I displays the sheet carrier concentration and Hall mobility for unannealed samples irradiated with 6 and 8 kJ m^{-2}, as well as a control sample. Sheet carrier concentration is calculated from the Hall voltage using the relationship $n_s = IB(qV_{Hall})^{-1}$. Samples irradiated with fluences below

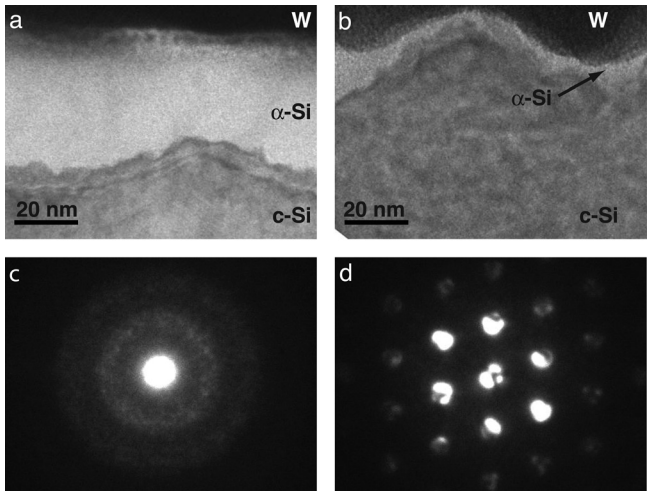

FIG. 3. Cross-sectional bright field TEM images of laser-doped (8 kJ m^{-2}) silicon reveal that (a) an amorphous layer (α–Si) resting atop the crystalline (c-Si) substrate directly after laser-irradiation and that (b) recrystallization occurs following a 30-min thermal anneal (975 K). The tungsten is deposited during FIB sample preparation. Microdiffraction confirms that single-pulse laser-doping produces (*c*) an amorphous surface resting atop (d) the monocrystalline substrate. Thermal annealing yields significant recrystallization of the amorphized volume.

6 kJ m^{-2} do not provide sufficient optical contrast to isolate and contact the sample, so data are unavailable for those samples. The Hall coefficient is negative for all samples and changes by four orders of magnitude following laser irradiation, with a sheet carrier density equal to approximately 1% of sulfur dopants for both samples irradiated at both 6 and 8 kJ m^{-2}.

In Figure 4, the current-voltage relationship of the junction between the laser-doped region and the substrate is shown before and after thermal annealing. Rectifying behavior of the expected polarity for a *p-n* junction (in which the laser-doped region and substrate act as the n- and p-regions, respectively) is observed in annealed samples.

B. Large area doping

The goal of this experiment was to extend the single-pulse doping experiments by fabricating a large-area of fs-laser hyperdoped silicon. This system serves as a bridge between the easily studied single-pulse system and large-area, roughened material that has been studied previously. After laser-exposure, the surface retains a mirror-like appearance. Atomic force microscopy indicates a root mean-square

TABLE I. Summary of Hall effect measurements shown alongside the sulfur dose (measured with SIMS). Where not marked, all quantities are ±1 in the last significant digit except fluence, which is subject to a 20% uncertainty.

Laser fluence (kJ m^{-2})	Dose Φ (10^{13} cm^{-2})	Sheet carrier concentration n_s (10^{11} cm^{-2})	Mobility μ_H ($cm^2/V\,s$)	$\frac{n_s}{\Phi} \times 10^2$
Control	n/a	-1.7×10^{-4}	1450	—
4	3	n/a	n/a	—
6	5	−3.0	830	0.6 ± 0.3
8	3	−3.1	690	1.2 ± 0.6

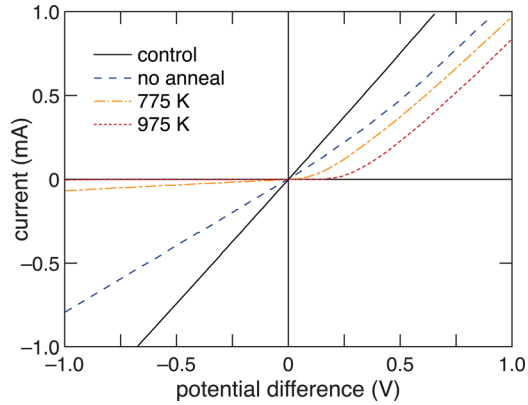

FIG. 4. Current-voltage properties of the junction between the laser-doped region (8 kJ m^{-2}) and the p-type substrate (polarity of measurement shown in Fig. 1(a)). Current-voltage properties are linear directly following laser-irradiation, but exhibit rectification following a thermal anneal, indicating activation of the sulfur donors, and/or healing of the junction defects.

surface roughness of 2.5 ± 0.5 nm (Figure 5(a)); the unexposed areas of the wafer exhibit a roughness of 0.28 ± 0.01 nm. The bright-field TEM image is shown in Figure 5(b) and confirms that the surface has little or no surface roughness. Selected area diffraction (Figure 5(b), inset) and high resolution TEM (Figure 5(c)) indicate that the laser-melted region—or at least its upper portion—resolidifies in an amorphous phase. Analysis of TEM images from six different areas reveals the amorphous layer extends 66 ± 7 nm from the surface.

The sulfur concentration-depth profile is shown in Figure 5(d). The concentration of sulfur near the surface is at least 6×10^{19} cm^{-3} and remains above crystalline silicon's solid solubility limit (10^{16} cm^{-3}) up to a distance of 90 ± 14 nm from the surface, when it falls below the measurement limit due to oxygen contamination. The total sulfur dose is $(2.8 \pm 0.2) \times 10^{14}$ cm^{-2}.

IV. DISCUSSION

The primary goal of these experiments is to develop new fs-laser hyperdoping techniques that eliminate surface roughness, enabling the study of fs-laser hyperdoping using high-precision structural and electrical measurements. Specifically, we seek to isolate the hyperdoped region in geometries amenable to characterization techniques such as quantified SIMS and Hall effect. These characterization tools are necessary for developing and testing predictive models of fs-laser hyperdoping, and we discuss initial observations enabled by these measurements.

The heat-flow dynamics following fs-laser melting are complex due to the variety of non-equilibrium conditions that follow the absorption of the laser pulse.[6,7] The data reported above enable us to describe several aspects of the melting and resolidification dynamics. Following laser-induced melting, silicon resolidifies as thermal energy diffuses from the molten layer into the substrate. The structure of the resolidified layer depends on the velocity at which the resolidification front moves through the molten layer; for example, the maximum velocity that can be tolerated for crystalline regrowth is about 15 m s^{-1}.[18] The TEM images for both the single-pulse

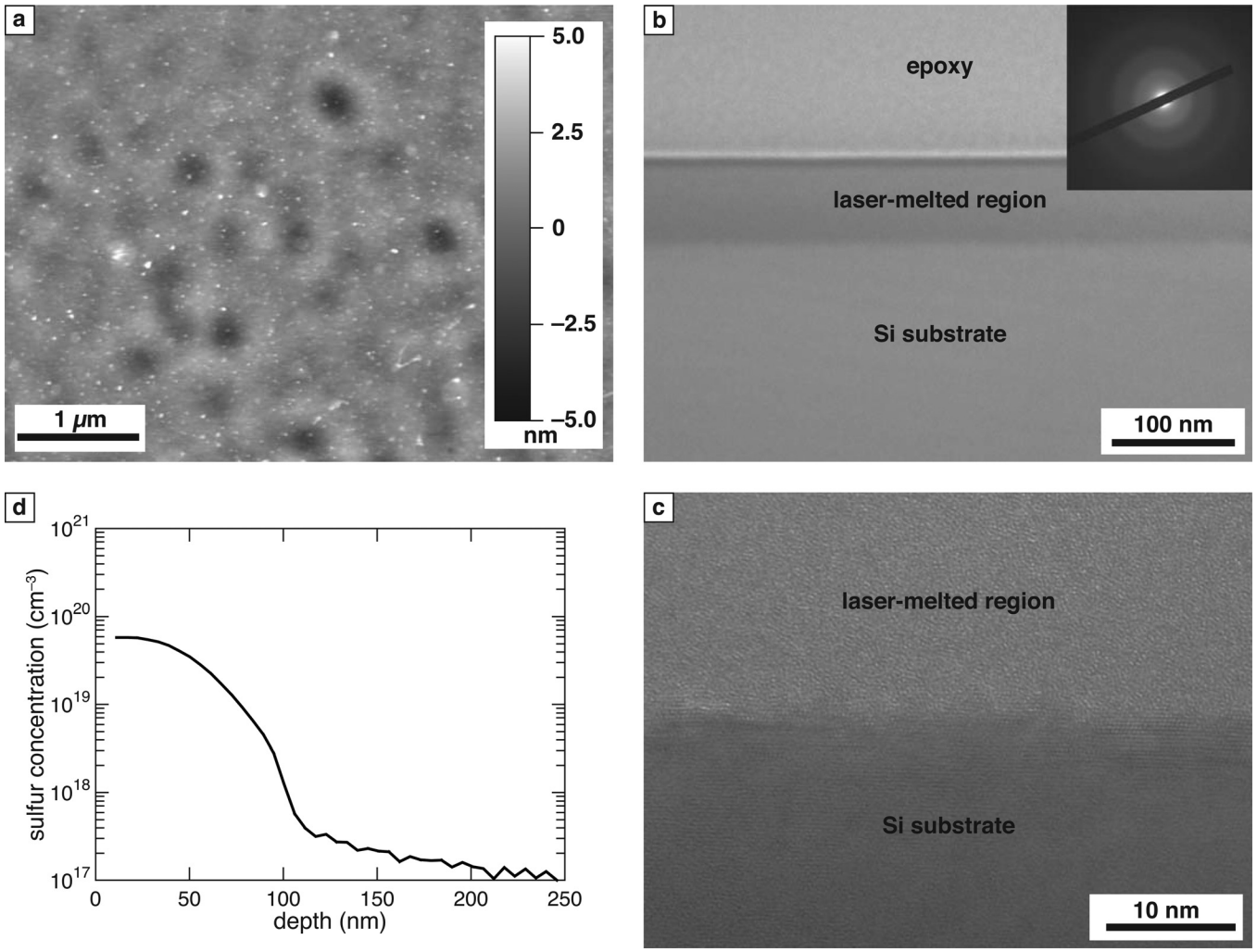

FIG. 5. Chemical and structural characterization of laser-hyperdoped silicon. (a) Atomic force microscope image of the laser-irradiated surface. (b) Bright-field TEM image showing an amorphous silicon layer extending 66 ± 7 nm from the surface, with the crystalline substrate underneath. Inset shows selected area diffraction of the laser-melted region inset. (c) Depth profile of the sulfur concentration. The measured concentration exceeds the solid solubility limit of sulfur in crystalline silicon at depths no greater than 90 ± 14 nm. (d) High-magnification TEM image revealing the amorphous and crystalline interference patterns of the surface region and substrate, respectively.

samples (Figure 3) as well as the large area sample (Figure 5(b)) reveal an amorphous layer extending 45–75 nm from the sample surface. These images provide a lower bound on melt depth (which extends to at least the amorphous-layer depth) and also indicate that the resolidification-front velocity exceeded 15 m s^{-1} in these regions. The transient reflectance measurements indicate that the melt duration during the single-pulse experiment was (8 ± 2) ns. Because the melt depth is at least 45 nm, this measurement indicates an *average* resolidification velocity of at least (6 ± 2) m s^{-1}. Comparing to the peak velocity of 15 m s^{-1}, this measurement indicates that the resolidification-front exhibits a range of velocities, as expected.[19]

Although the exact mechanism through which sulfur is dissolved into the silicon melt is not clear from this experiment, we can offer a hypothesis: SF_6 molecules irradiated by fs-laser pulses dissociate,[20] and sulfur atoms that dissolve into the laser-melted silicon layer are trapped by the high-velocity resolidification front. The data available from SIMS, transient reflectance, and TEM all support this hypothesis. Using the melt duration $(8 \pm 2$ ns) and literature values of sulfur diffusivity in molten silicon,[21] we calculate an upper bound on the diffusion length of sulfur in the molten silicon to be about 40 nm. Comparing to Figure 2(a), this estimate appears reasonable given that sulfur is concentrated in the upper 20 nm (and noting that only the surface of the laser-melted region is liquid for the entire melt duration; deeper portions of the laser-melted silicon resolidify earlier). After the sulfur diffuses a short distance from the surface, the resolidification front (exhibiting a peak velocity 15 m s^{-1}) traps a high concentration of sulfur in the resolidified amorphous-silicon layer. The estimated peak and average resolidification-front velocities are well in excess of that necessary for significant solute trapping,[22] explaining the high concentrations of sulfur in our samples. The sulfur concentration in the large-area sample exhibits a deeper, broader distribution with both a higher peak concentration and areal density of dopants. Without a detailed model of dopant incorporation, the evolution from single-laser pulse doping (Figure 2) to the results of Figure 5 cannot be explained. However, for the large area sample of Figure 5, all points on the surface were exposed to approximately 15 laser pulses,

so it is reasonable that a greater concentration of sulfur would be distributed to greater depths. We note that the SIMS profiles indicate that the sulfur persists at non-equilibrium concentrations at depths below the amorphous layer. We expect that the laser-melted (and hyperdoped) region extends slightly deeper than the amorphous region, with initial resolidification occurring via epitaxial regrowth as the resolidification front accelerates up to $15\,\mathrm{m\cdot s^{-1}}$. Recoil of sulfur atoms from the primary ion beam during the SIMS measurement, though, could also account for some amount of broadening in the SIMS profile.[23]

The measured value of the melting threshold ($2.1 \pm 0.5\,\mathrm{kJ\cdot m^{-2}}$) is comparable to reports under similar conditions,[24] but measurable quantities of sulfur are not observed until the laser fluence is approximately twice the melting threshold (4 *vs.* $2\,\mathrm{kJ\cdot m^{-2}}$). The lack of measured sulfur just above the melting threshold is likely due to lack of sufficient signal-to-noise to resolve its presence. For example, the melt duration and depth precisely at the melting threshold will both be vanishingly small, limiting the quantity of sulfur that can dissolve into the molten layer and the signal measured during SIMS. We note that the role of fluorine was not investigated in this study, as previous work has shown that it does not affect the optical and electronic properties of sulfur-hyperdoped silicon;[25] however, some fluorine is likely present as well.[4]

The presence of mostly amorphous silicon in the laser-melted region is in contrast to previous publications involving irradiation with many laser pulses above the ablation threshold; under those conditions, the laser-hyperdoped region exhibits a polycrystalline structure.[10,26] Other authors have previously noted that silicon irradiated with ultrashort pulses resolidifies in either an amorphous or crystalline phase depending on the fluence, and that only a relatively narrow fluence range exists in which crystallinity can be recovered.[27,28] Under laser-irradiation conditions that produce surface roughness, preferential reflection and focusing by surface features can produce spatially varying fluence patterns.[10,26] These substantially more complex laser-heating cycles could be responsible for the structural differences observed between this and previous work.

Isolated sulfur atoms introduce two occupied energy levels deep within the band gap of silicon and can thus act as an electron donor.[29] We have previously observed donor behavior in black silicon and exploited it to construct photodiodes.[1] The Hall-effect data of Table I indicate that sulfur dopants are electrically active immediately following the doping process. Indeed, the measured sheet-carrier concentration n_s increases by a factor exceeding 10^4 following irradiation, indicating that approximately $(1.2 \pm 0.6)\%$ of the sulfur donors are ionized. Assuming that all sulfur dopants are on substitutional sites (which introduces a donor level 318 meV below the conduction band edge[29]), semiconductor statistics dictate that about 0.6% of the sulfur states would be ionized,[30] in reasonable agreement with measurements. However, the measured carrier mobility is quite high for an amorphous layer, suggesting that the crystalline layer below the amorphous region may play a role in electron transport. The presence of amorphous and crystalline conducting layers introduces uncertainty into analysis of electronic transport measurements, and the Hall coefficient is anomalous under certain conditions in amorphous silicon.[31]

The uncertainty in interpreting the Hall effect data motivated measurement of the *I–V* properties of the junction between the laser-doped region and the substrate. Directly following irradiation, the *I–V* properties between the laser-doped region and the substrate are linear and do not reflect donor activity by the sulfur dopants. However, the junction begins to exhibit nonlinear *I–V* properties after annealing, with strong rectification after annealing at 975 K. The TEM image of the annealed sample (Figure 3(b)), however, reveals that the amorphous silicon has recrystallized following this thermal treatment. Unfortunately, it is not possible to collect Hall effect data from an annealed sample as the laser-irradiated SOI samples are mechanically unstable under annealing. Thus, it remains unclear if the onset of rectification with annealing is due to additional donor activation or the improvement of crystal and junction quality. Regardless of whether rectification depends upon structural or electronic changes, though, it is clear that annealing is necessary to form a rectifying junction.

Focusing now on the AFM result of Figure 5(a), we note that electromagnetic waves reflect in a specular fashion from a surface of average roughness σ when their wavelength λ satisfies $\lambda \gg \sigma$.[32] The large-area sample meets this criterion for all visible wavelengths, with the AFM measurement revealing a surface roughness of 2.5 ± 0.5 nm. The laser-exposed regions are somewhat rougher than the original wafer surface (0.28 ± 0.01 nm), but this increase is not significant enough to impact the other characterization techniques we describe. Thus, we successfully demonstrate the ability to eliminate surface optically relevant roughness during fs-laser hyperdoping. The fluence necessary to observe both laser-doping as well as smooth resolidified surfaces is somewhat lower than might be expected given the single pulse experiments, which indicate that a fluence of $4\,\mathrm{kJ\cdot m^{-2}}$ is necessary to achieve significant doping. Irradiation with multiple pulses is known to lower modification thresholds such as melting and ablation;[28] additionally, the smaller laser spot used for this experiment introduces relatively large error bars into the fluence measurement.

V. CONCLUSION

In conclusion, we present fundamental structural and electronic properties of silicon doped via fs-laser irradiation, using two different experimental techniques for eliminating surface roughness from fs-laser hyperdoping. We report basic structural characteristics with higher quantitative accuracy than previously possible, including the dopant profile and dopant electrical activation measured via SIMS and the Hall effect, respectively. Specifically, we report the properties of silicon doped with sulfur via a single fs-laser pulse, establishing processes and observations to serve as a baseline for future development of a detailed model of fs-laser hyperdoping. Further, we demonstrate a non-roughening fabrication method for large area fs-laser hyperdoping. This fabrication technique similarly facilitates high-accuracy

characterization. These methods and data will be useful for developing a predictive model of fs-laser hyperdoping and, therefore, extending the capabilities of the technique.

ACKNOWLEDGMENTS

Several people contributed to this work. M.W. conceived the experiment, fabricated the samples, carried out the electronic characterization, and carried out SIMS measurements. M.W. and M.-J.S. analyzed the data and prepared the manuscript. M.-J.S. acquired the AFM data, and Y.-T.L. performed the transient reflectance measurement. M.S. (supervised by S.G.) and H.Z. prepared the TEM images, and E.M. supervised the research. The authors wish to acknowledge Tom Mates (UCSB) for assisting with the SIMS, with support from the National Science Foundation (NSF) Contract DMR 04-20415. The authors are indebted to Professor Michael Aziz for helpful discussions, as well as to him and Brion Bob for providing the data for correcting and normalizing the SIMS data. This work was performed in part at Harvard University's Center for Nanoscale Systems, a member of the National Nanotechnology Infrastructure Network, which is supported by the NSF. The NSF supported this work under Contracts CBET-0754227 and DMR-0934480. M.S. acknowledges support from the Chesonis Family Foundation; M.W. acknowledges support from the NSF Graduate Research Fellowship program.

[1]J. E. Carey, C. H. Crouch, M. Shen, and E. Mazur, Opt. Lett. **30**, 1773 (2005).
[2]A. J. Said, D. Recht, J. T. Sullivan, J. M. Warrender, T. Buonassisi, P. D. Persans, and M. J. Aziz, Appl. Phys. Lett. **99**, 073503 (2011).
[3]A. Luque and A. Martí, Adv. Mater. **22**, 160 (2010).
[4]R. Younkin, J. E. Carey, E. Mazur, J. A. Levinson, and C. M. Friend, J. Appl. Phys. **93**, 2626 (2003).
[5]M. A. Sheehy, B. R. Tull, C. M. Friend, and E. Mazur, Mater. Sci. Eng. B **137**, 289 (2007).
[6]M. Sher, M. T. Winkler, and E. Mazur, MRS Bull. **36**, 439 (2011).
[7]B. R. Tull, J. E. Carey, E. Mazur, J. P. McDonald, and S. M. Yalisove, MRS Bull. **31**, 626 (2006).
[8]C. Wu, C. H. Crouch, L. Zhao, J. E. Carey, R. Younkin, J. A. Levinson, E. Mazur, R. M. Farrell, P. Gothoskar, and A. Karger, Appl. Phys. Lett. **78**, 1850 (2001).
[9]T. Her, R. J. Finlay, C. Wu, S. Deliwala, and E. Mazur, Appl. Phys. Lett. **73**, 1673 (1998).
[10]V. Zorba, N. Boukos, I. Zergioti, and C. Fotakis, Appl. Opt. **47**, 1846 (2008).
[11]Y. Peng, Y. Wen, D. S. Zhang, S. D. Luo, L. Chen, and Y. M. Zhu, Appl. Opt. **50**, 4765 (2011); Y. Liu, S. Liu, Y. Wang, G. Feng, J. Zhu, and L. Zhao, Laser Phys. **18**, 1148 (2008).
[12]B. K. Nayak, V. Iyengar, and M. Gupta, Prog. Photovolt. **19**, 631 (2011).
[13]T. G. Kim, J. M. Warrender, and M. J. Aziz, Appl. Phys. Lett. **88**, 241902 (2006); M. Tabbal, T. G. Kim, D. N. Woolf, B. Shin, and M. J. Aziz, Appl. Phys. A **98**, 589 (2010); P. Carey, T. W. Sigmon, R. L. Press, and T. S. Fahlen, IEEE Electron Device Lett. **EDL-6**, 291 (1985).
[14]M. J. Aziz and T. Kaplan, Acta Metall. **36**, 2335 (1988); J. A. Kittl, P. G. Sanders, M. J. Aziz, D. P. Brunco, and M. O. Thompson, Acta Mater. **48**, 4797 (2000).
[15]We use "RCA" or "Standard clean" for silicon, as described in W. Kern, *Handbook of Semiconductor Wafer Cleaning Technology* (Noyes, Park Ridge, 1993). Briefly: first, soak for 10 min in a 1:1:5 solution of NH_4OH:-H_2O_2:H_2O at 80 °C; then for 30 s in a 5% HF solution; third, for 10 min in a 1:1:6 solution of HCl:H_2O_2:H_2O at 80 °C; and finally for 30 s in a 5% HF solution.
[16]L. J. van der Pauw, Philips Tech. Rev. **20**, 220 (1958).
[17]M. Y. Shen, C. H. Crouch, J. E. Carey, and E. Mazur, Appl. Phys. Lett. **85**, 5694 (2004).
[18]M. O. Thompson, J. W. Mayer, A. G. Cullis, H. C. Webber, N. G. Chew, J. M. Poate, and D. C. Jacobson, Phys. Rev. Lett. **50**, 896 (1983).
[19]P. Lorazo, L. Lewis, and M. Meunier, Phys. Rev. B **73**, 134108 (2006).
[20]J. H. Sanderson, R. V. Thomas, W. A. Bryan, W. R. Newell, P. F. Taday, and A. J. Langley, J. Phys. B **30**, 4499 (1997).
[21]K. Tang, E. J. Øvrelid, G. Tranell, and M. Tangstad, JOM **61**, 49 (2009).
[22]M. J. Aziz in *Laser Surface Treatment of Metals*, edited by C. W. Draper and P. Mazzoldi (Martinus Nijhoff, Dordrecht, Netherlands, 1986), p. 649.
[23]K. Wittmaack, Vacuum **34**, 119 (1984).
[24]D. P. Korfiatis, K.-A. Th Thoma, and J. C. Vardaxoglou, J. Phys. D **40**, 6803 (2007).
[25]M. A. Sheehy, L. Winston, J. E. Carey, C. M. Friend, and E. Mazur, Chem. Mater. **17**, 3582 (2005).
[26]C. H. Crouch, J. E. Carey, J. M. Warrender, M. J. Aziz, E. Mazur, and F. Y. Genin, Appl. Phys. Lett. **84**, 1850 (2004).
[27]P. L. Liu, R. Yen, N. Bloembergen, and R. T. Hodgson, Appl. Phys. Lett. **34**, 864 (1979).
[28]J. Bonse, S. Baudach, J. Krüger, W. Kautek, and M. Lenzner, Appl. Phys. A **74**, 19 (2002).
[29]E. Janzén, R. Stedman, G. Grossmann, and H. G. Grimmeiss, Phys. Rev. B **29**, 1907 (1984).
[30]Using Eq. (322.4) of J. S. Blakemore, *Semiconductor Statistics* (Dover, New York, 1987), we implemented a depth-dependent calculation that accounts for the depth distribution of the sulfur.
[31]N. F. Mott, Philos. Mag. Part B **63**, 3 (1991).
[32]J. Strutt (Rayleigh), *The Theory of Sound* (Macmillan, London, 1877), Ch. 12, Vol. 2.